Biochemistry

Article

pubs.acs.org/biochemistry

Characterization of Protein Tyrosine Phosphatase 1B Inhibition by Chlorogenic Acid and Cichoric Acid

James M. Lipchock,[*,†] Heidi P. Hendrickson,[‡] Bonnie B. Douglas,[†,‡] Kelly E. Bird,[†,‡] Patrick S. Ginther,[†,‡] Ivan Rivalta,[⊥,‡] Nicholas S. Ten,[‡] Victor S. Batista,[*,‡] and J. Patrick Loria[*,‡,§]

[†]Department of Chemistry, Washington College, Chestertown, Maryland 21620, United States

[‡]Department of Chemistry, Yale University, New Haven, Connecticut 06511, United States

[⊥]Univ Lyon, Ens de Lyon, CNRS, Université Lyon 1, Laboratoire de Chimie UMR 5182, F-69342, Lyon, France

[§]Department of Molecular Biophysics and Biochemistry, Yale University, New Haven, Connecticut 06511, United States

Supporting Information

ABSTRACT: Protein tyrosine phosphatase 1B (PTP1B) is a known regulator of the insulin and leptin signaling pathways and is an active target for the design of inhibitors for the treatment of type II diabetes and obesity. Recently, cichoric acid (CHA) and chlorogenic acid (CGA) were predicted by docking methods to be allosteric inhibitors that bind distal to the active site. However, using a combination of steady-state inhibition kinetics, solution nuclear magnetic resonance experiments, and molecular dynamics simulations, we show that CHA is a competitive inhibitor that binds in the active site of PTP1B. CGA, while a noncompetitive inhibitor, binds in the second aryl phosphate binding site, rather than the predicted benzfuran binding pocket. The molecular dynamics simulations of the apo enzyme and cysteine−phosphoryl intermediate states with and without bound CGA suggest CGA binding inhibits PTP1B by altering hydrogen bonding patterns at the active site. This study provides a mechanistic understanding of the allosteric inhibition of PTP1B.

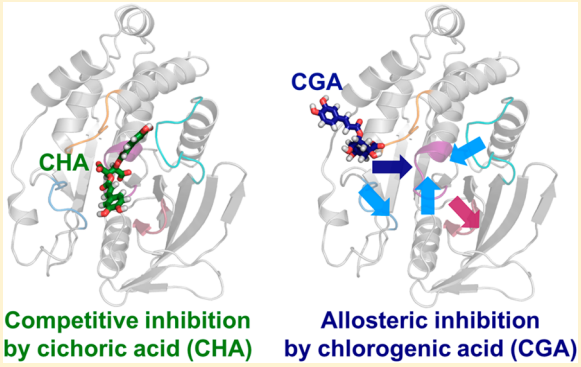

Protein tyrosine phosphatases (PTPs) play an important role in maintaining cellular health by regulating phosphotyrosine (pY) levels. Disruption of normal catalytic activity results in a myriad of diseases, including diabetes, cancer, inflammation, and obesity.[1−3] There are more than 100 known human PTPs,[4] all of which share similar three-dimensional structures despite varying degrees of sequence identity.[5] The hallmark of a PTP is the P-loop consensus sequence, $C(X)_5RS/T$, which is essential for phosphotyrosine binding and catalysis.[3,5] Specifically, the arginine residue in the P loop aids binding of the substrate by forming hydrogen bonds with the phosphoryl oxygen atoms, while the cysteine is responsible for nucleophilic attack of the phosphoryl moiety to form a thiophosphoryl bond in the first step of catalysis. A conserved aspartic acid located on the flexible acid (or so-called WPD) loop protonates the tyrosine leaving group. The thiophosphoryl intermediate is hydrolyzed in a subsequent step by a water molecule activated by a second proton transfer involving the same aspartate in the acid loop. Both reaction steps require a flexible acid loop capable of adopting an open conformation to allow substrate binding and a closed conformation that facilitates cleavage and hydrolysis.[5−10]

One member of the PTP family is protein tyrosine phosphatase 1B (PTP1B), which plays an important role in insulin and leptin signaling. In insulin signaling, PTP1B is known to dephosphorylate the activated insulin receptor and insulin receptor substrates to attenuate the cellular response to insulin binding.[11−14] In the leptin signaling pathway, PTP1B dephosphorylates Janus kinase 2, which is normally phosphorylated in response to leptin binding to the leptin receptor to trigger a feeling of satiety.[15,16] Mice with PTP1B gene knockouts have enhanced insulin sensitivity and low body weight, even when fed a high-fat diet.[17] For these reasons, PTP1B has become an active therapeutic target for the treatment of type II diabetes and obesity.

While PTP1B inhibitors with nanomolar affinity have been identified, no ligands have progressed beyond phase II clinical trials.[1,18] Therapeutics that function as competitive inhibitors are hindered by the need for anionic charge, as evidenced by the fact that tyrosine-containing substrates have little affinity for PTP1B unless they are phosphorylated.[19,20] Unfortunately, this negative charge reduces cell permeability and targets the active-site region of PTP1B, a region with the highest degree of similarity to other known PTPs, resulting in diminished selectivity.[18] Conversely, a study of 22 representative PTPs has shown that the remaining surface of PTP1B has diverse

Received: October 6, 2016
Revised: December 13, 2016
Published: December 13, 2016

Downloaded via YALE UNIV on March 8, 2019 at 16:13:31 (UTC).
See https://pubs.acs.org/sharingguidelines for options on how to legitimately share published articles.

© 2016 American Chemical Society

DOI: 10.1021/acs.biochem.6b01025
Biochemistry 2017, 56, 96−106

features, despite a shared three-dimensional architecture.[5] This suggests that the greatest promise for the design of selective, cell-permeable therapeutics targeting PTP1B exists for non-competitive inhibitors that bind outside the enzyme active site. To this end, Wiesmann and co-workers identified a series of benzfuran-based ligands that allosterically inhibit PTP1B by binding distal to the active site near the C-terminal tail.[21] The resulting crystal structure in the presence of one of these analogues revealed the acid loop in the open conformation, suggesting a potential mechanism for allosteric inhibition is the inhibition of acid-loop closure.[21] Krishnan et al. characterized binding of a distinct inhibitor (MSI-1436), which bound to the disordered PTP1B C-terminal tail as well as α-7 and showed some overlap with the benzfuran binding site.[22] Recently, Baskaran and co-workers utilized docking and molecular dynamics simulations to predict that cichoric acid (CHA) and chlorogenic acid (CGA) bind in the same location as the benzfuran analogues and inhibit PTP1B by altering acid-loop dynamics, suggesting the benzfuran pocket may be a target with broad utility for the design of potential therapeutics.[23]

In this study, we have combined computational and experimental methods to investigate the mechanism by which CHA and CGA inhibit PTP1B. Through the use of inhibition kinetics, nuclear magnetic resonance (NMR) titrations, and extensive molecular dynamics simulations, we have determined that the binding modes and functions of these ligands are distinctly different from those of the benzfuran analogues. In addition, we provide structural information about the ligand-bound complexes through the aid of docking simulations using restraints from the NMR ligand titrations that further support distinct modes of action.

EXPERIMENTAL PROCEDURES

Materials. CHA and CGA were purchased from Sigma-Aldrich (St. Louis, MO). For labeled protein expression, deuterium oxide was purchased from Cambridge Isotope Laboratories (Tewksbury, MA) and [^{15}N]ammonium chloride and [$^{13}C_6$]-D-glucose were purchased from Sigma-Aldrich.

Protein Expression and Purification. PTP1B was expressed and purified as previously described.[22,24] The WT PTP1B 1−301 amino acid construct was used for all experiments described below. This PTP1B protein was expressed in *Escherichia coli* BL21(DE3) cells in medium containing 100 μg/mL ampicillin (LB expression) or carbenicillin (M9 expression). For isotopic enrichment for NMR experiments, cells were grown in M9 minimal medium supplemented with [^{15}N]ammonium chloride (1.0 g/L) and [$^{13}C_6$]-D-glucose (2.0 g/L), as necessary. All NMR samples were perdeuterated by growth and expression in minimal medium containing 99% D_2O. For NMR studies, pure protein fractions were dialyzed into 50 mM HEPES (pH 6.8) with 150 mM NaCl, 0.5 mM TCEP, 7% D_2O, and 0.02% NaN_3 (NMR buffer) and concentrated to 0.2−0.4 mM.

PTP1B Inhibition Assay. Steady-state kinetic parameters were measured for PTP1B using *p*-nitrophenyl phosphate (pNPP, 0.5−40 mM) as the substrate in NMR buffer. The rate of reaction was calculated by monitoring the change in absorbance at 405 nm where the molar absorbance for pNPP under these conditions is 12600 M^{-1} cm^{-1}. Kinetic parameters were determined by fitting the reaction rates to different inhibition models as a function of the inhibitor and pNPP concentrations using GraphPad Prism version 6.0d. The total reaction volume in all cases was 500 μL, and the temperature was maintained at 25 °C using a water-regulated cuvette holder. The reaction was initiated by adding 10 μL of ∼25 μM protein for a final concentration of ∼0.5 μM PTP1B. The concentration of CGA was varied from 0.0 to 6.6 mM by adding 100 μL of serially diluted CGA in NMR buffer. The concentration of CGA was confirmed using the molar absorbance at 332 nm in ethanol (20030 M^{-1} cm^{-1}).[25] The concentration of CHA was determined gravimetrically and varied from 0.0 to 4.0 mM by adding 50 μL of serially diluted CHA in NMR buffer.

Lineweaver−Burke plots (not shown) of CHA inhibition intersected on the *y*-axis consistent with competitive inhibition. Therefore, these data were fit with eq 1. CGA inhibition kinetics were fit to a noncompetitive (eq 2) inhibition model.

$$v = \frac{V_m[S]}{K_m(1 + [I]/K_i) + [S]} \quad (1)$$

$$v = \frac{V_m[S]}{K_m(1 + [I]/K_i) + [S](1 + [I]/K_i)} \quad (2)$$

where v is the measured enzyme-catalyzed reaction rate (velocity), K_m is the Michaelis constant, K_i is the inhibition constant, and [S] and [I] are the concentrations of the substrate and inhibitor, respectively.

NMR Assignments. Two-dimensional ^{1}H−^{15}N HSQC spectra were assigned on the basis of published data deposited in the BMRB (entries 5474, 19224, and 25375).[22,26,27] Assignments were confirmed from a TROSY-HNCACB experiment conducted at 19 °C on a Varian 600 MHz spectrometer.

NMR Titrations with CGA and CHA. NMR chemical shift perturbations of PTP1B resonances due to binding of CHA and CGA were monitored by acquiring a series of ^{1}H−^{15}N TROSY spectra of ^{15}N- and ^{2}H-labeled PTP1B upon addition of increasing concentrations of CHA and CGA. For CHA, spectra were recorded at 0.00, 0.20, 0.40, 1.00, 3.00, and 5.00 mM CHA from a 150 mM CHA stock into 0.38 mM [^{15}N,^{2}H]PTP1B (550 μL starting volume). For CGA, spectra were recorded at 0.00, 0.11, 0.21, 0.52, 1.04, 5.20, and 8.32 mM CGA using a 156 mM CGA stock titrated into 0.38 mM [^{15}N,^{2}H]PTP1B (550 μL starting volume). To identify regions with significant chemical shift perturbations, composite (^{1}H and ^{15}N) chemical shifts were calculated as follows:

$$\Delta\delta\ (\text{ppm}) = \sqrt{\left(\delta_{HN}{}^2 + \frac{\delta_N{}^2}{25}\right)/2} \quad (3)$$

where δ_{HN} and δ_N are the changes in amide proton and nitrogen chemical shifts, respectively, from the initial resonance positions in the absence of any added ligand.[28] Residues exhibiting $\Delta\delta$ values greater than twice the standard deviation of the 10% trimmed mean value (2σ) were classified as significant chemical shifts for further analysis. These shifts were fit globally to eq 4 to obtain the apparent dissociation constant (K_d) for CGA or CHA binding.

DOI: 10.1021/acs.biochem.6b01025
Biochemistry 2017, 56, 96−106

$$\Delta\delta = 0.5\Delta\delta_{max}\left[1 + X + \frac{K_d}{[PTP1B]} - \sqrt{\left(1 + X + \frac{K_d}{[PTP1B]}\right)^2 - 4X}\right] \quad (4)$$

where $\Delta\delta_{max}$ is the maximal chemical shift observed for each residue and X is the CHA:PTP1B or CGA:PTP1B ratio at each titration point.

HADDOCK Inhibitor Docking. Molecular structures for CHA and CGA were optimized using *ab initio* Hartree−Fock energy minimizations with a 3-21G* basis set in Spartan'14.[29] These ligands were docked into apo PTP1B [Protein Data Bank (PDB) entry 2HNP][6] using the HADDOCK2.2 web portal.[30,31] Solvent accessible residues that experience significant chemical shifts upon addition of an inhibitor were selected as "active residues" for the docking simulations. Passive residues were selected automatically by the program. For CHA, the following active residues were utilized: R45, S118, L119, G183, V184, C215, G218, Q262, T263, A264, D265, and Q266. For CGA, the following active residues were utilized: R24, H25, D48, V49, I219, M258, G259, and Q262.

Molecular Dynamics Simulations. Molecular dynamics (MD) simulations were performed using the AMBER-ff14SB force field as implemented in the NAMD software package.[32] To determine the binding sites of CHA and CGA, the crystal structure of apo PTP1B (PDB entry 2HNP) was used as the initial structure.[6] Evidence that CGA acts as a noncompetitive inhibitor (discussed below) suggests that CGA further slows the rate-limiting step of catalysis (i.e., the hydrolysis of the thiophosphoryl intermediate). To understand the effect of CGA on this second catalytic step, the crystal structure of PTP1B with a vanadate intermediate (PDB entry 3i80) was used as the initial structure for MD simulations.[33] In the simulations, a phosphoserine residue was used to model the phosphocysteine intermediate, and for both apo and CGA-bound PTP1B simulations, residue Csv215 was replaced with Sep. Importantly, the vanadate−cysteine complex has a vanadate oxygen (O4) that is coordinated by Q262 and D181, which may represent the position of the water molecule necessary for hydrolysis. The coordinated vanadate oxygen (O4) was replaced with a water residue (HOH) to maintain the natural orientation of residues in the initial structure.

Two independent trajectories were analyzed for each of the following five systems: apo PTP1B (2HNP), CHA-bound, CGA-bound, the apo thiophosphoryl intermediate, and CGA bound to the thiophosphoryl intermediate (3i80). In all simulations with CHA or CGA bound, an optimal docked pose was used as the initial position for each ligand. Force field parameters for each ligand are provided in the Supporting Information, as determined from the generalized AMBER force field (GAFF). The protein was capped using the zwitterionic N-terminus and C-terminus. Hydrogens and approximately 13000 TIP3P water molecules were added to each system using the AmberTools15 software package.[34]

Each system was equilibrated in the *NPT* ensemble prior to production runs. First, the positions of hydrogen atoms and water molecules were optimized while the protein and ligand heavy atom positions were constrained to their respective crystal structure or docked-pose positions. Next, the systems were slowly heated to 298 K in the *NVT* ensemble using Langevin dynamics. During the initial heating steps, harmonic constraints were applied to the protein and ligand heavy atoms and gradually released with an increasing temperature. Finally, the systems were equilibrated in the *NPT* ensemble at 298 K and 1.0 atm using the Langevin piston. Long-range electrostatic interactions were taken into account using the particle mesh Ewald method, and van der Waals interactions were calculated using a switching distance of 10.0 Å and a cutoff of 12.0 Å. The integration time step was 1 fs. The duration of production runs following equilibration was 50 ns for calculations of binding positions. The duration of production runs following equilibration was 20 ns for calculations to determine the effect of CGA on conformational dynamics in the phosphoryl intermediate configuration.[35]

Analysis of MD simulations, including characterization of binding-site hydrogen bonds and hydrophobic contacts, was conducted using the VMD software package in combination with in-house scripts.[36] Hydrogen bonds during the trajectory were determined using the VMD HBonds Plugin, with the usual cutoff values of 3.0 Å between heavy atoms and a <20° bond angle. Pearson correlation coefficients for the number of unique hydrogen bonds formed for each residue at each picosecond frame of the trajectories were calculated to understand changes in hydrogen bond networks due to ligand binding. Changes in hydrogen bond networks upon ligand binding were determined (1) by the number of hydrogen bonds formed between unique atom pairs and (2) by the correlation between the number of unique hydrogen bonds formed per picosecond for each residue.

Chemical shifts were calculated using SHIFTX2.[37] For apo, CHA-bound, and CGA-bound systems, amide N and H chemical shifts were calculated for the protein at each picosecond of the trajectory and averaged over both independent trajectories. The composite amide chemical shifts were determined according to eq 3. Chemical shift perturbations ($\Delta\delta$) were calculated by taking the difference between the average ligand-bound and apo composite amide chemical shift for each residue. The normalized deviations from the mean composite chemical shift perturbation were calculated according to eq 5 to highlight the residues that experience significant perturbations.

$$\Delta\delta_\sigma\ (\text{ppm}) = \frac{|\Delta\delta - \langle\Delta\delta\rangle|}{\sigma} \quad (5)$$

RESULTS

PTP1B Inhibition Assay. PTP1B inhibition kinetics were measured for the ligands CHA and CGA. Profiles for the catalyzed reaction rate versus the pNPP (substrate) concentration are shown in Figure 1. Both CHA and CGA are weak binding inhibitors. Fitting with the competitive inhibition equation (eq 1) to the experimental data for CHA yielded the following kinetic parameters: k_{cat} = 7.00 ± 0.07 s^{-1}, K_m = 2.8 ± 0.1 mM, and K_i = 1.44 ± 0.08 mM (Table 1). For CGA, the noncompetitive model yielded the following kinetic parameters: k_{cat} = 8.2 ± 0.1 s^{-1}, K_m = 3.3 ± 0.1 mM, and K_i = 8.2 ± 0.4 mM (Table 1).

NMR Titration with CHA. To determine the location of inhibitor binding, [^{15}N,^{2}H]PTP1B was titrated with increasing CHA concentrations ranging from 0 to 5.0 mM. Composite chemical shift perturbations ($\Delta\delta$) were calculated and plotted for each residue (Figure 2a, left). The following residues had chemical shift perturbations at least two standard deviations

DOI: 10.1021/acs.biochem.6b01025
Biochemistry 2017, 56, 96−106

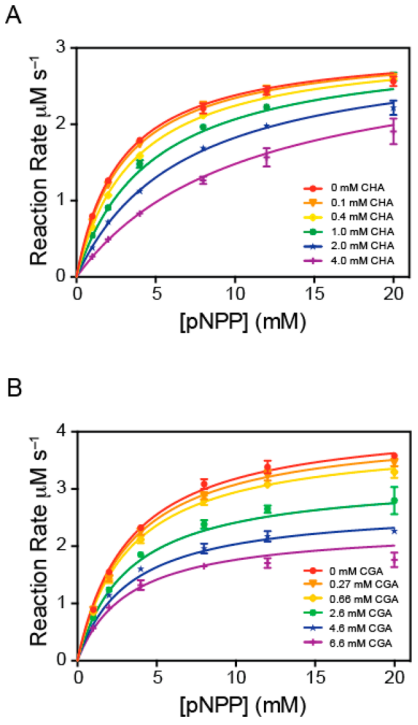

Figure 1. Inhibition kinetics for PTP1B with CHA. Reaction rates were measured for pNPP concentrations ranging from 2 to 20 mM for each inhibitor concentration. Inhibitor concentrations were varied (A) from 0.0 to 4.0 mM for CHA and (B) from 0.0 to 6.6 mM for CGA. Error bars are obtained from triplicate measurements.

Table 1. PTP1B Inhibition Kinetic Parameters for CHA and CGA

	k_{cat} (s^{-1})	K_m (mM)	K_i (mM)[a]	K_d (mM)[b]
CHA	7.0 ± 0.1	2.8 ± 0.1	1.4 ± 0.1	1.6 ± 0.2
CGA	8.2 ± 0.1	3.3 ± 0.1	8.2 ± 0.4	1.5 ± 0.2

[a]Value obtained from steady-state kinetics. [b]Value obtained from NMR chemical shift titrations.

from the 10% trimmed mean: R45, F182, G183, V184, C215, G218, G223, I261, T263, A264, D265, and Q266. In addition, several residues were broadened significantly such that their peak intensity was reduced by >80% of their original value: Q85, G86, I219, and Q262. The broadening of NMR resonances is consistent with millisecond time scale chemical exchange from a weak binding ligand. Overlays for the NMR spectra for the entire protein and residues experiencing significant changes in chemical shift are shown in Supplemental Figures 1A and 2. The chemical shifts for residues experiencing statistically significant perturbations were analyzed as a function of CHA concentration to determine the apparent affinity of CHA for PTP1B. The chemical shifts for residues listed above were fit globally using eq 5 and gave an apparent dissociation constant for CHA (K_d = 1.6 ± 0.2 mM) for binding to PTP1B (Supplemental Figure 3). This value is virtually identical to its kinetically determined K_i value. To identify the location of binding, the amide nitrogens for these residues were highlighted on the structure of PTP1B (PDB entry 2HNP)[6] as large colored spheres. These residues are clustered around the active site, specifically the P loop, the WPD loop, and the Q loop (residues 256–264) (Figure 2a, middle), consistent with the competitive inhibition model determined by steady-state kinetics.

NMR Titration with CGA. Similar to CHA, CGA was titrated into [^{15}N,^{2}H]PTP1B at concentrations ranging from 0 to 8.3 mM. Several residues exhibited chemical shift perturbations that were two standard deviations or more from the 10% trimmed mean value: E26, V49, I219, M258, G259, L260, and T263 (Figure 3a, left). Overlays of NMR spectra for the entire protein and individual residues are shown in Supplemental Figures 1B and 4. Residues with statistically significant chemical shift perturbations were analyzed as a function of CGA concentration to determine the apparent affinity of CGA for PTP1B. When the NMR titration data for these residues were fit globally, a K_d of 1.5 ± 0.2 mM for binding of CGA to PTP1B was obtained (Supplemental Figure 5). This value is approximately 5-fold tighter than the K_i value determined by steady-state kinetic analysis. The amino acid residues with significant CGA binding-induced perturbations are identified as colored spheres on the PTP1B structure (Figure 3a, middle). These residues are clustered around helix 2, the pTyr loop, and the Q loop adjacent to the active site. The distinction of these residues from active-site residues is consistent with the noncompetitive mode of inhibition for CGA determined from steady-state kinetic measurements.

Docking CHA into PTP1B. To gain insight into the binding mode of the competitive inhibitor, CHA was docked into PTP1B (PDB entry 2HNP)[6] using the HADDOCK2.2 web portal.[30,31] Solvent accessible residues with significant perturbations in chemical shift or broadening were utilized as restraints for HADDOCK docking as described above. The simulations yielded six structural clusters. These clusters with the following HADDOCK scores are as follows: −109.3 ± 2.3 (120 structures, z score of −1.7), −92.6 ± 6.5 (25 structures, z score of −0.9), −74.6 ± 8.9 (12 structures, z score of −0.1), −56.3 ± 9.9 (6 structures, z score of 0.8), −55.7 ± 5.9 (7 structures, z score of 0.8), and −52.4 ± 3.7 (13 structures, z score of 1.0). The first cluster is most statistically relevant given the large number of structures in the cluster and the significantly lower HADDOCK score. The docked conformation used as the initial configuration for MD simulations is shown in Figure 2a (right). This figure highlights that CHA binding is consistent with the observed chemical shift perturbations from the NMR titration because CHA makes contacts with the residues that have the largest chemical shift perturbations or broadening, specifically the P loop, the WPD loop, and the Q loop. This binding pocket is highlighted in a surface view of PTP1B shown in Figure 4a. A close-up view of the active site overlaid with the phosphopeptide-bound structure (PDB entry 1PTT)[7] reveals that one of the central carboxylic acid groups in CHA appears to mimic the substrate's phosphoryl group by binding to catalytic-site residues in the P loop (Figure 4b). In particular, the CHA carboxylic acid group reproduces the distances between the substrate phosphoryl group and Cys215 (2.81 Å) and also forms similar hydrogen bond contacts with the R221 guanidinium group (Figure 4c). Additional lowest-energy conformations for CHA are shown in Supplemental Figure 6. In all cases, CHA adopts a similar orientation and makes contacts with the P loop, the WPD loop, and the Q loop.

CGA Docking into PTP1B. To determine the structure of CGA-bound PTP1B, solvent accessible residues with significant perturbations in chemical shift or broadening were utilized as restraints for HADDOCK docking into PTP1B (PDB entry

DOI: 10.1021/acs.biochem.6b01025
Biochemistry 2017, 56, 96−106

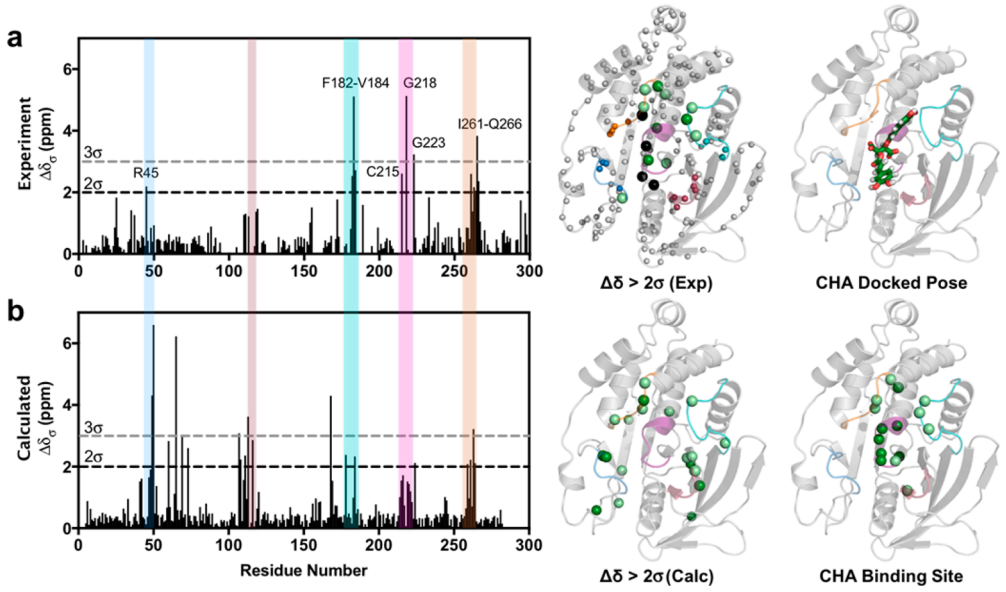

Figure 2. Chemical shift analysis and structural mapping for the titration of [^{15}N]PTP1B with CHA. PTP1B loops involved in catalysis are highlighted as follows: the phosphotyrosine binding P loop (magenta), the WPD loop (cyan), the Q262 loop (orange), the pTyr46 loop (blue), and the E115 loop (rose). (a) Normalized composite amide chemical shift perturbations (left) upon the addition of 5.0 mM CHA for each assigned amide resonance. Statistically significant chemical shift perturbations (middle) upon addition of 5.0 mM CHA are mapped onto PTP1B (PDB entry 2HNP).[6] Amides with composite shifts greater than 3 standard deviations from the mean upon titration with CHA are shown as large dark green spheres. Amides that shift 2−3σ from the mean are shown as large light green spheres. Amides that are broadened >80% are shown as large black spheres. Assigned amides that do not experience significant changes in chemical shift or intensity are shown as small gray spheres. Docked pose of CHA (green sticks, right) used as the starting configuration for MD simulations. (b) Calculated normalized composite amide chemical shift perturbations (left) as determined by the difference between average amide chemical shifts from MD simulations of CHA-bound and apo PTP1B. Statistically significant calculated chemical shift perturbations (middle) are mapped onto PTP1B (PDB entry 2HNP), with the same color coding as in panel a. Residues within 5.0 Å of CHA during the MD trajectories (right) mapped onto PTP1B (PDB entry 2HNP). Residues within 5.0 Å of CHA for at least 75% of trajectory frames are shown as light green spheres and for 100% of trajectory frames as dark green spheres.

2HNP).[6] The simulations yielded seven structural clusters. These clusters with the following HADDOCK scores are as follows: −61.3 ± 2.4 (131 structures, z score of −1.4), −58.8 ± 5.2 (6 structures, z score of −1.2), −48.2 ± 3.5 (11 structures, z score of −0.5), −40.0 (4 structures, z score of 0.2), −33.9 ± 2.6 (20 structures, z score of 0.6), −27.6 ± 4.9 (8 structures, z score of 1.1), and −25.6 ± 2.0 (4 structures, z score of 1.2). The first cluster is most statistically relevant given the large number of structures in the cluster and the more negative HADDOCK score. The four lowest-energy conformations are shown in Figure 5. Figure 3a (right) highlights that CGA binding is consistent with the observed chemical shift perturbations for the NMR titration, as the residues with the largest changes in chemical shift form the binding pocket. This binding pocket is highlighted in a surface view of PTP1B in Figure 5a. A close-up view of binding and active sites reveals that in three of the four conformations the quinic acid portion of CGA binds in a pocket formed between the pTyr loop and Q loop, and the caffeic portion of CGA interacts with helix 2 (Figure 5b). This binding site is consistent with the secondary aryl-phosphate binding site in the phosphotyrosine-bound PTP1B crystal structure (PDB entry 1PTY).[38,39] The overlay in Figure 5b highlights the agreement between CGA-docked poses and the pTyr substrate in the secondary binding site (PDB entry 1PTY). The CGA carboxyl group overlaps well with the position of the substrate phosphoryl group. In one of the four lowest-energy conformations, the quinic acid portion of CGA is rotated in the pocket formed by the pTyr loop and the Q loop, and the caffeic acid moiety interacts with the pTyr loop and not helix 2.

Molecular Dynamics Simulations of CHA-Bound PTP1B. Molecular dynamics simulations were performed to gain mechanistic insight into the binding effects of CHA. First, the NMR chemical shifts were calculated for each picosecond of the simulation and averaged. The areas of largest chemical shift changes from the apo structure occur in protein regions also identified by the NMR experiments (Figure 2b). The calculated chemical shift perturbations upon CHA binding indicate significant perturbations occur in the key catalytic-site loops. Residues with significant chemical shift perturbations are shown as spheres in Figure 2b (middle) and include H60, A69, K73, V108, N111, K116, T178, V184, C226, G259, I261, and A264 ($\Delta\delta$ between 2σ and 3σ from the mean) and V49, S50, N65, V107, V113, T168, and T263 ($\Delta\delta$ greater than 3σ from the mean). Chemical shift calculations are based only on the protein structure at each frame in the trajectory; thus, the effect of the ligand is included indirectly, and slight differences between calculated and measured residues are expected. The calculations presented here capture the effect of the ligand-induced conformational and dynamical changes quite well, as the residues with significant calculated shift perturbations that are located outside of the active-site regions are also within the second sphere of the active site and form hydrogen bond interactions with residues in the P loop. Therefore, the MD simulations are expected to serve as a relevant model for understanding interactions between CHA and PTP1B.

The CHA binding site predicted by MD simulations remains in agreement with the site identified by the measured chemical shift perturbations upon CHA binding (Figure 2b, right). The calculated binding site is based on residues possessing heavy

DOI: 10.1021/acs.biochem.6b01025
Biochemistry 2017, 56, 96−106

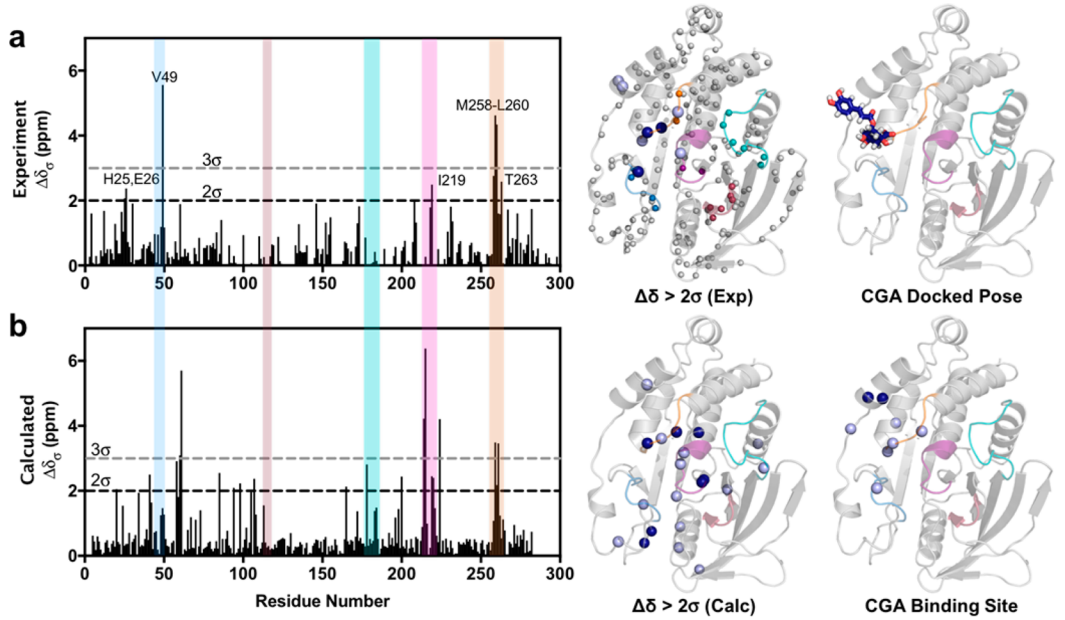

Figure 3. Chemical shift analysis and structural mapping for the titration of [^{15}N]PTP1B with CGA. PTP1B loops involved in catalysis are highlighted as follows: the phosphotyrosine binding P loop (magenta), the WPD loop (cyan), the Q262 loop (orange), the pTyr46 loop (blue), and the E115 loop (rose). (a) Normalized composite amide chemical shift perturbations (left) upon addition of 8.0 mM CGA for each assigned amide resonance obtained from eq 5. Statistically significant chemical shift perturbations (middle) upon addition of 8.0 mM CGA are mapped onto PTP1B (PDB entry 2HNP).[6] Amides with composite shifts greater than 3 standard deviations from the mean upon titration with CGA are shown as large dark blue spheres. Amides that shift 2−3σ from the mean are shown as large light blue spheres. Assigned amides that do not experience significant changes in chemical shift or intensity are shown as small gray spheres. Docked pose of CGA (dark blue sticks, right) used as the starting configuration for MD simulations. (b) Calculated normalized composite amide chemical shift perturbations (left) due to CGA binding. Statistically significant calculated chemical shift perturbations (middle) are mapped onto PTP1B (PDB entry 2HNP), with the same color coding as in panel a. Residues within 5.0 Å of CGA during the MD trajectories (right) are mapped onto PTP1B (PDB entry 2HNP). Residues within 5.0 Å of CGA for at least 65% of trajectory frames are shown as light blue spheres and for at least 95% of trajectory frames as dark blue spheres.

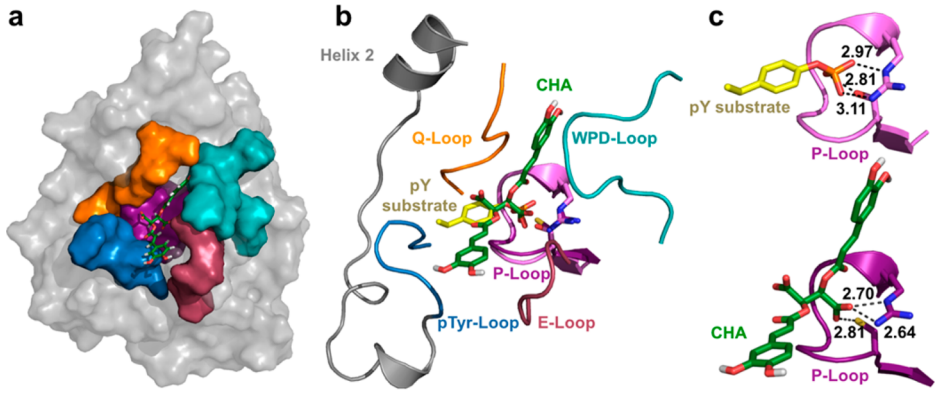

Figure 4. Analysis of CHA-bound PTP1B from HADDOCK docking.[30,31] (a) Surface structure of CHA-docked PTP1B. CHA is shown as green sticks. PTP1B loops are highlighted as follows: the P loop (magenta), the WPD loop (cyan), the Q262 loop (orange), the pTyr46 loop (blue), and the E115 loop (rose). (b) Overlay of phosphopeptide-bound PTP1B (PDB entry 1PTT)[7] and the structure obtained from HADDOCK docking CHA into PTP1B (PDB entry 2HNP).[6] The phosphopeptide (pY substrate) is shown as yellow sticks. (c) Orientation of the pY substrate (top) in 1PTT[7] highlighting the distance (in angstroms) between phosphate oxygens and PTP1B S215 and R221. Orientation of CHA in the docked pose (bottom), highlighting the distance (in angstroms) between carboxylate oxygens and PTP1B C215 and R221 atoms.

atoms within 5.0 Å of CHA for the entire trajectory, including C215, A217, G218, I219, G220, R221, and Q266. Flexibility of CHA within the binding pocket is captured by considering residues interacting with CHA for most of the trajectory frames (e.g., at least 75%), including K120, F182, G183, V184, S216, Q262, T263, and N265. The CHA caffeic moiety bound between the pTyr loop and E115 loop is more flexible than the moiety bound among the P loop, the WPD loop, and the Q loop. This moiety forms hydrogen bonds with D48 in the pTyr loop and is also capable of forming hydrogen bonds with E-loop residues. On the other hand, the CHA carboxylate groups form consistent hydrogen bond interactions with P-loop amides, including A217, I219, G220, and R221. Likewise, the caffeic hydroxyl groups among the P loop, the WPD loop, and the Q loop form consistent hydrogen bonds with residues Q262 and N265 in the Q loop. Additional CHA binding information is shown in Supplemental Figure 7A. Overall, the

DOI: 10.1021/acs.biochem.6b01025
Biochemistry 2017, 56, 96−106

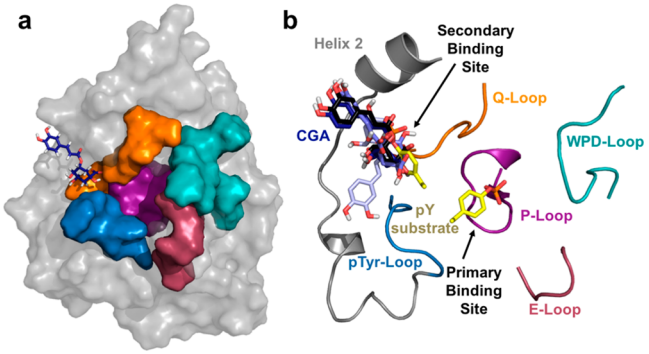

Figure 5. Analysis of CGA-bound PTP1B from HADDOCK docking.[30,31] (a) Surface structure of CGA-docked PTP1B. CGA is shown as dark blue sticks. PTP1B loops are highlighted as follows: the P loop (magenta), the WPD loop (cyan), the Q262 loop (orange), the pTyr46 loop (blue), and the E115 loop (rose). (b) Overlay of phosphotyrosine-bound PTP1B (PDB entry 1PTY) and the structure obtained from HADDOCK docking CGA into PTP1B (PDB entry 2HNP).[6] The phosphotyrosines (pY substrate) from PDB entry 1PTY are shown as yellow sticks. The four lowest-energy conformations for CGA in the largest cluster are shown as sticks (black for the lowest and light blue for the highest).

MD simulations provide evidence that supports CHA as a competitive inhibitor that binds in the catalytic site of PTP1B.

Molecular Dynamics Simulations of CGA-Bound PTP1B. Molecular dynamics simulations were also performed on the CGA-bound PTP1B to provide an atomistic understanding of the allosteric effect of CGA on the catalytic site. Calculated composite chemical shift perturbations are in agreement with measured shifts, with most significant shifts located among helix 2, the pTyr loop, and the Q loop (Figure 3b). Residues with significant chemical shift perturbations are shown as spheres in Figure 3b (middle) and include Q21, K41, K58, Q85, H94, M98, V107, T165, T178, E200, I219, G220, and L260 ($\Delta\delta$ between 2σ and 3σ from the mean) and H60, Q61, H214, C215, T224, G259, and I261 ($\Delta\delta$ greater than 3σ from the mean). The residues with significant calculated shift perturbations are more widely distributed than those with significant measured perturbations; however, chemical shift predictions are based only on the protein residues, and the differences may be related to direct ligand effects. Overall, the good overlap between calculated and measured chemical shifts over the full MD trajectory, provides evidence that the simulations will provide insight into the CGA binding interactions and their allosteric inhibition of PTP1B catalysis.

The CGA binding site consistent with the MD simulations is shown in Figure 3b (right). The calculated binding site is based on residues having heavy atoms within 5.0 Å of CGA for most of the trajectory frames, R24 and H25. The CGA caffeic hydroxyl and carboxyl oxygens form consistent hydrogen bonds with residues in helix 2, including Y20, R24, and D29. The MD simulations confirm the flexibility of CGA in the binding pocket, and residues that interact with CGA for at least 65% of trajectory frames include D29, D48, R254, M258, G259, and Q262. (Additional CGA binding information is provided in Supplemental Figure 7B.) The residues in the binding pocket confirm that CGA binds in the PTP1B second aryl-phosphate binding site and therefore acts as an allosteric inhibitor.

Allosteric Effect of CGA on PTP1B Hydrolysis. To determine the allosteric mechanism by which CGA inhibits PTP1B catalysis, further MD simulations were performed to investigate the effect of CGA on the PTP1B phosphoryl–cysteine intermediate. Experimental evidence indicates CGA acts as a noncompetitive inhibitor and does not affect substrate binding. Furthermore, the simplest explanation for the effect of CGA is that it further slows the rate-determining step of the reaction, which is hydrolysis of the phosphoryl–cysteine intermediate.[33] Hydrolysis occurs via a water molecule coordinated by Q262 and D181, and favorable oreintation of these residues has been confirmed in crystal structures that model the hydrolysis transition state (PDB entry 3i80).[33] Comparison of the simulations between the enzyme–phosphoryl intermediate structure and CGA bound to PTP1B at the phosphoryl intermediate stage (Sep215) indicates that the CGA affects hydrogen bonding and coordination of waters within the catalytic site via multiple allosteric networks.

MD simulations reveal that fewer water molecules are present in the PTP1B catalytic site on average when CGA is bound. The number of water molecules in the catalytic site is related to the distance between residues D181 and Q262, as shown in Figure 6. (Additional information is presented in Supplemental Figure 8.) In the apo PTP1B simulations, the distance between the Q262 ε-nitrogen and D181 carboxylate oxygen fluctuates around three values (4.9, 6.5, and 8.7 Å), as shown in Figure 6A. CGA does not affect the Q262–D181

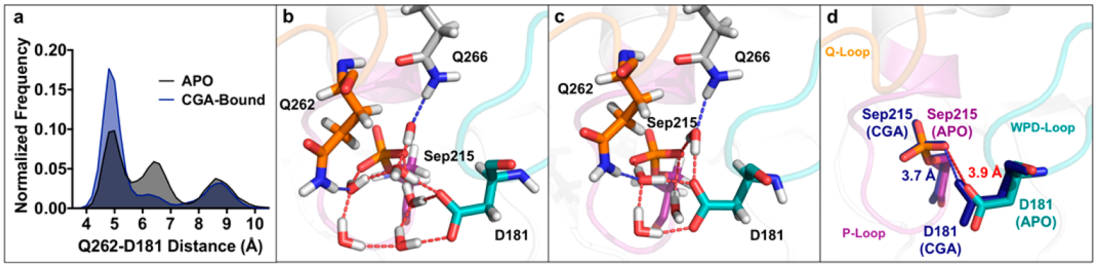

Figure 6. Effect of CGA on the hydrogen bond configuration within the catalytic site. (a) Histogram of the distance distributions between the Q262 ε-nitrogen atom and the closest D181 carboxylate oxygen atom for each picosecond frame of apo (gray) and CGA-bound (dark blue) trajectories. There are three primary distributions between these atoms for the apo enzyme and two primary distributions for the CGA-bound enzyme. (b) Snapshot from the apo simulation showing the hydrogen bond configuration with a distance of 6.3 Å between the D181 oxygen atom and the Q262 nitrogen atom. (c) Snapshot from the CGA-bound simulation showing the hydrogen bond configuration with a distance of 4.9 Å between D181 oxygen and Q262 nitrogen atoms. (d) Average positions of D181 and Sep215 determined from apo (teal) and CGA-bound (dark blue) simulations. The D181 carboxylate group is 0.2 Å closer on average to the phosphoryl intermediate when CGA is bound. PTP1B loops involved in catalysis are highlighted as follows: P loop (magenta), WPD loop (cyan), and Q262 loop (orange).

DOI: 10.1021/acs.biochem.6b01025
Biochemistry 2017, 56, 96–106

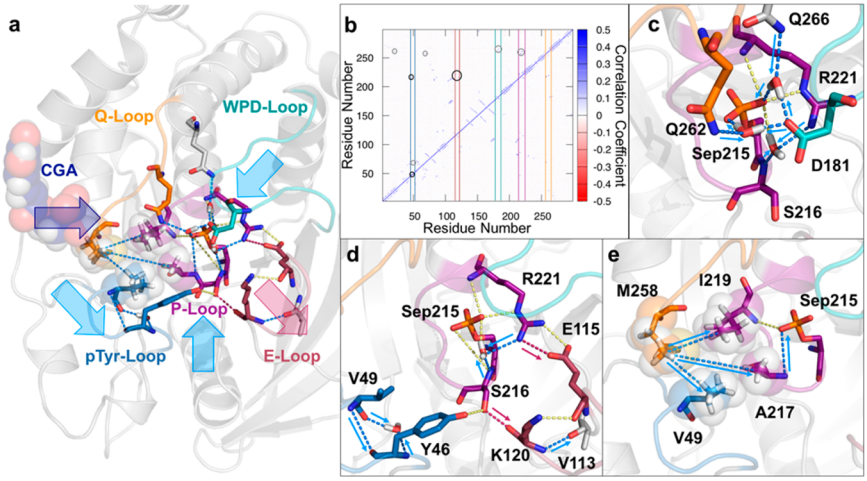

Figure 7. Analysis of the effect of CGA on PTP1B allosteric pathways. PTP1B loops are highlighted as follows: P loop (magenta), WPD loop (cyan), Q262 loop (orange), pTyr46 loop (blue), and E115 loop (rose). Dotted lines and arrows indicate changes in distances (ΔR) between hydrogen bonds or side chain hydrophobic groups upon CGA binding [light blue for shorter ($\Delta R < -0.1$ Å), yellow for no change (-0.1 Å $< \Delta R < 0.1$ Å), and light red for longer ($\Delta R > 0.1$ Å)]. (a) Overview of allosteric networks affected by CGA binding (dark blue spheres). CGA effectively "pushes" the hydrophobic groups of M258 toward the active site (dark blue arrow), resulting in a compact hydrogen bond configuration at the active site. (b) Correlations in the number of hydrogen bonds formed per residue. Key correlations between PTP1B loops (color-coded vertical lines) are highlighted by gray circles. Black circles specify correlations affected by CGA binding. Changes in average distance upon CGA binding for hydrogen bonds spanning (c) the catalytic site, (d) the P loop, pTyr loop, and E loop, (e) and the P loop via changes in hydrophobic group distances across the pTyr loop and Q loop (hydrophobic groups highlighted as spheres).

distance distribution at large distances. At Q282−D181 distances of ∼8.7 Å, more water molecules can enter the catalytic site because the Q262 side chain rotates away from D181 to form hydrogen bonds with the G259 backbone carbonyl. CGA can form hydrogen bonds with Q262 when it binds (as shown in Supplemental Figure 7B), but these interactions occur while Q262 is rotated away from the active site and do not affect the large distance distribution. On the other hand, the average distance between Q262 and D181 decreases by 0.55 Å when CGA is bound. Significant changes to the distribution occur at shorter distances, where compact configurations with Q262−D181 distances of around 4.9 Å are more likely than open configurations with distances around 6.5 Å when CGA is bound. These results indicate that the presence of CGA causes the compact hydrogen bond configurations to become more favorable than open configurations.

Figure 6b shows a representative hydrogen bonding configuration within the catalytic site for apo PTP1B. In this structure, the Q262−D181 distance is 6.3 Å and waters within 5.0 Å of the Sep215 residue are shown. The Sep215 phosphate groups coordinate one water molecule directly with each of the D181, Q262, and Q266 residues. These water molecules collectively coordinate one central water molecule, and D181 and Q262 coordinate two additional waters along the periphery of the active site. The hydrogen bond configuration shown in Figure 6c represents the 4.9 Å configuration, which is more probable when CGA is bound. In this configuration, Q262 and Q266 each continue to coordinate one water molecule with the phosphate group; however, the central water is no longer present. Instead, D181 takes the place of the central water by coordinating the waters directly to phosphate oxygen atoms with Q262 and Q266, and D181 no longer coordinates its original mutual water molecule with phosphate groups. Furthermore, the D181 backbone becomes significantly more rigid when CGA is bound (Supplemental Figure 9), and the average distance between D181 and the phosphate groups decreases by 0.2 Å (Figure 6d). Overall, these effects indicate stronger hydrogen bonding interactions occur within the catalytic site when CGA is bound. It is expected that these interactions cause the nucleophilic attack of the phosphate group by water to become less favorable and therefore are responsible for hydrolysis inhibition.

Examination of allosteric pathways surrounding the CGA binding site reveals that CGA disrupts key networks connected to the catalytic site. An overview describing the allosteric effect of CGA on the PTP1B catalytic site is provided in Figure 7a (distances are provided in Supplemental Table 1). In general, CGA creates disruptions within the hydrophobic pocket comprising its binding site, pushing M258 toward hydrophobic residues in the pTyr loop and P loop. These disruptions break the hydrogen bond network connecting the pTyr loop, P loop, and E loop and strengthen interactions within each loop, which leads to a preference for a compact hydrogen bond network within the catalytic site.

To determine the allosteric pathways that couple the PTP1B catalytic loops, correlations between the numbers of unique hydrogen bonds formed for each residue were considered for each residue pair (Figure 7b). Large positive correlation coefficients indicate formation of hydrogen bonds is correlated between residues (e.g., when two residues form a mutual hydrogen bond, or when they form hydrogen bonds with a mutual water molecule). Large negative coefficients indicate hydrogen bonding is competitive between two residues (i.e., when one residue forms a hydrogen bond, a hydrogen bond to the other residue breaks). The correlation matrix in Figure 7b highlights several highly positively correlated residue pairs that connect the catalytic-site loops, including Y46 and V49, Y46 and S216, K120 and S216, E115 and R221, V49 and N68, N68 and R257, A217 and R257, G218 and R257, F182 and T263, and G183 and Q266. Of these pairs, CGA binding has the greatest effect on correlations and hydrogen bond distances between Y46 and V49, Y46 and S216, K120 and S216, and E115 and R221. Correlations that connect the CGA binding-site residues to the Q loop and P loop include Y20 and I261,

DOI: 10.1021/acs.biochem.6b01025
Biochemistry 2017, 56, 96−106

and I219 and I261; however, these correlations and hydrogen bond distances are not greatly affected by CGA.

Changes to the hydrogen bond network within the catalytic site upon CGA binding are shown in Figure 7c. The average distances between D181 and residues Q262, Q266, and Sep215 become shorter upon CGA binding. Notably, the distance between S216 and R221 nitrogen atoms also decreases. Figure 7c shows that the water molecule typically coordinated between D181 and Sep215 moves away from D181 and becomes coordinated by S216 and R221 as the hydrogen bond configuration becomes more compact. Stabilization of this water molecule away from D181 by S216 and R221 explains how the compact hydrogen bond configuration can become stabilized with respect to the more open configuration typically found during the apo simulations.

The S216 and R221 residues are able to effectively coordinate the water molecule in the active site due to changes in the allosteric network that occur when CGA binds (Figure 7d). For instance, the V49 residue becomes much closer to the Y46 residue, which disrupts the connection among the pTyr loop, the P loop, and the E loop and enhances connections within each loop. The disruption creates two key breaks in the hydrogen bond network (K120 and S216, and E115 and R221) that allow S215 and R221 to form more stable hydrogen bonds with the mutual water molecule.

These key disruptions to the hydrogen bond network can be traced back to the CGA ligand. The CGA binding site is located around a hydrophobic pocket formed by M258 (Q loop), V49 (pTyr loop), and A217 and I219 (P loop) residues. When CGA binds, M258 is pushed an average of 0.22 Å closer to these other residues in the hydrophobic network (Figure 7e). Changes in hydrophobic interactions affect the orientation of V49, which in turn leads to changes in the hydrogen bond network in Figure 7d. In addition, A217 and I219 are hydrogen bonded to the phosphate group via backbone nitrogen atoms. Enhanced interactions with M258 decrease the distance between A217 and the phosphate groups, although there is no change with respect to I219. The shorter A217−phosphate distance is also related to the shorter S216−R221 distances and is likely to contribute to stabilization of the compact hydrogen bond configuration within the catalytic site.

DISCUSSION

Given its role in the insulin and leptin signaling pathways, PTP1B remains an active target for the design of inhibitors that function as therapeutic agents for the treatment of type II diabetes and obesity. To date, the design of selective, cell-permeable inhibitors has been rather unsuccessful. To aid future drug design efforts, we have investigated the function of two ligands, CHA and CGA, predicted by molecular dynamics simulations to be allosteric inhibitors of PTP1B. The results of our inhibition assay with pNPP demonstrate clear competitive inhibition of PTP1B with CHA, which is validated by NMR chemical shifts changes in and around the catalytic P loop upon titration with CHA. When we use these shifted residues as restraints for ligand docking simulations, we obtain a ligand-bound structure consistent with competitive inhibition of PTP1B by CHA. As shown in Figure 4c, one of the central carboxylic acid functional groups in CHA overlays with the site normally occupied by the phosphoryl moiety in the substrate-bound structure (PDB entry 1PTT) with nearly perfect alignment. Furthermore, molecular dynamics simulations based on the docked configuration confirm the CHA interacts consistently with residues located in the catalytic site. This supports a mechanism in which CHA inhibits PTP1B function by directly blocking access to the catalytic site. Contrary to the molecular dynamics predictions in previous studies, we observe no significant chemical shift perturbations in the benzfuran binding pocket to support the idea that CHA inhibits PTP1B noncompetitively.[21,22]

Consistent with expectations, CGA was shown to non-competitively inhibit PTP1B through steady-state inhibition kinetics; however, the location of binding appears to be a binding pocket adjacent to the active site and not at the benzfuran pocket as evidenced by the lack of chemical shift perturbations to residues located in the benzfuran binding site (Figure 5a). All shifted residues are located in a binding pocket comprised of helix 2, the pTyr loop, and the Q loop adjacent to the active site. Docking simulations including all of the shifted resonances as restraints support a binding mode in which the quinic acid portion of CGA binds in the pocket comprised of the pTyr loop and Q loop; however, variance in the orientation of the caffeic acid moiety of CGA suggests that this portion of the molecule may bind less specifically and adopt multiple conformations when bound. The binding location of CGA, as well as its relative flexibility within the binding site, is confirmed by molecular dynamics simulations. Several of the H bond disruptions, observed by NMR chemical shifts and MD simulations, caused by CGA binding are critical for enzymatic function. In particular, mutation of Y46, E115, and R257, all conserved residues, results in 10^2−10^3-fold decreases in enzymatic activity.[39]

Curiously, we were not able to replicate the published EC_{50} values for inhibition by CHA and CGA. The inhibition kinetic data we measured yielded a K_i of 1.4 ± 0.1 mM for CHA and a K_i of 8.2 ± 0.4 mM for CGA, contrary to approximate EC_{50} values in the range of 10 μM from log-based inhibition concentrations at a single pNPP concentration.[23] Our kinetic values are more consistent with the K_d values measured by NMR titration analysis: 1.6 ± 0.2 mM for CHA and 1.5 ± 0.2 mM for CGA. It was discovered through the course of the inhibition assay that CHA and CGA absorb strongly at 405 nm at elevated pH values. It is not clear if the previously published kinetics measured enzyme inhibition using a base quench method frequently utilized for pNPP kinetics. If so, this could explain the discrepancies between the inhibition assay results. For our studies, all ligand solutions were prepared in a buffer identical to that used in the final PTP1B purification step and matched the pH with microliter additions of acid or base. Rather than utilizing a NaOH quench method, reaction rates were measured from the change in absorbance over the linear range in the first 2 min of the reaction. It is not known if the previously published kinetics utilized an organic solvent to dissolve the ligands, which may have also affected the inhibition assay. That work also used a PTP1B construct containing an additional 21-residue disordered C-terminal tail, whereas we used the shorter construct in our work.

Overall, the changes in hydrogen bonding within the catalytic site induced by CGA binding are expected to affect the mechanism for hydrolysis. Previous studies indicate that Q262 flexibility is required to obtain the correct orientation of Q262, D181, water, and phosphate groups within the catalytic site to allow for nucleophilic attack on the phosphate group by a water molecule.[40] While CGA binding does not appear to have a large effect on Q262 flexibility, our results do indeed point to the importance of the Q262−D181−water orientation in activating

DOI: 10.1021/acs.biochem.6b01025
Biochemistry 2017, 56, 96−106

hydrolysis. CGA binding disrupts the hydrophobic residues within the secondary aryl-phosphate binding site, which in turn causes disturbances in hydrogen bonds connecting the pTyr and E loops to the P loop. These changes stabilize a more compact hydrogen bond configuration within the catalytic site, causing hydrolysis to become less favorable. It is important to note that this mechanism of allosteric regulation for PTP1B is distinct from the mechanism utilized by the benzfuran analogues that bind distal to the active site, which function by modulating the conformation in the WPD loop. In this respect, future work toward designing effective allosteric PTP1B inhibition may focus on investigating how the orientation of water molecules and surrounding residues in the catalytic site can facilitate or inhibit hydrolysis.

■ ASSOCIATED CONTENT

Supporting Information

The Supporting Information is available free of charge on the ACS Publications website at DOI: 10.1021/acs.biochem.6b01025.

Nine figures containing experimental and MD results, one table containing H bond distances, and one table containing MD parameters for ligands CGA and CHA (PDF)

■ AUTHOR INFORMATION

Corresponding Authors

*Department of Chemistry, Washington College, 300 Washington Ave., Chestertown, MD 21620. E-mail: jlipchock2@washcoll.edu. Telephone: (410) 810-5081.

*Department of Chemistry, Yale University, 225 Prospect St., P.O. Box 208107, New Haven, CT 06511. E-mail: patrick.loria@yale.edu. Telephone: (203) 436-2518.

*Department of Chemistry, Yale University, 225 Prospect St., P.O. Box 208107, New Haven, CT 06511. E-mail: victor.batista@yale.edu. Telephone: (203) 432-6672.

ORCID

Heidi P. Hendrickson: 0000-0002-5012-738X

Ivan Rivalta: 0000-0002-1208-602X

J. Patrick Loria: 0000-0002-4824-9089

Funding

This work was supported by start-up funds allocated to J.M.L. by Washington College and National Institutes of Health Grants R01 GM112781 to J.P.L. and GM10621 awarded to V.S.B. This work used the Extreme Science and Engineering Discovery Environment (XSEDE), which is supported by National Science Foundation Grant ACI-1053575.

Notes

The authors declare no competing financial interest.

■ ACKNOWLEDGMENTS

V.S.B. acknowledges supercomputer time from the National Energy Research Scientific Computing Center (NERSC).

■ ABBREVIATIONS

PTP1B, protein tyrosine phosphatase 1B; CGA, chlorogenic acid; CHA, chichoric acid; EDTA, ethylenediaminetetraacetic acid; TCEP, tris(2-carboxyethyl)phosphine; CPMG, Carr−Purcell−Meiboom−Gill.

■ REFERENCES

(1) Barr, A. J. (2010) Protein tyrosine phosphatases as drug targets: strategies and challenges of inhibitor development. *Future Med. Chem. 2*, 1563−1576.

(2) Tautz, L., Critton, D. A., and Grotegut, S. (2013) Protein tyrosine phosphatases: structure, function, and implication in human disease. *Methods Mol. Biol. 1053*, 179−221.

(3) Tonks, N. K. (2006) Protein tyrosine phosphatases: from genes, to function, to disease. *Nat. Rev. Mol. Cell Biol. 7*, 833−846.

(4) Alonso, A., Sasin, J., Bottini, N., Friedberg, I., Friedberg, I., Osterman, A., Godzik, A., Hunter, T., Dixon, J., and Mustelin, T. (2004) Protein tyrosine phosphatases in the human genome. *Cell 117*, 699−711.

(5) Barr, A. J., Ugochukwu, E., Lee, W. H., King, O. N., Filippakopoulos, P., Alfano, I., Savitsky, P., Burgess-Brown, N. A., Muller, S., and Knapp, S. (2009) Large-scale structural analysis of the classical human protein tyrosine phosphatome. *Cell 136*, 352−363.

(6) Barford, D., Flint, A. J., and Tonks, N. K. (1994) Crystal-Structure of Human Protein-Tyrosine Phosphatase-1b. *FASEB J. 8*, A1322.

(7) Jia, Z. C., Barford, D., Flint, A. J., and Tonks, N. K. (1995) Structural Basis for Phosphotyrosine Peptide Recognition by Protein-Tyrosine-Phosphatase 1b. *Science 268*, 1754−1758.

(8) Liu, G. X., Tan, J. Z., Niu, C. Y., Shen, J. H., Luo, X. M., Shen, X., Chen, K. X., and Jiang, H. L. (2006) Molecular dynamics simulations of interaction between protein-tyrosine phosphatase 1B and a bidentate inhibitor. *Acta Pharmacol. Sin. 27*, 100−110.

(9) Peters, G. H., Frimurer, T. M., Andersen, J. N., and Olsen, O. H. (1999) Molecular dynamics simulations of protein-tyrosine phosphatase 1B. I. ligand-induced changes in the protein motions. *Biophys. J. 77*, 505−515.

(10) Peters, G. H., Frimurer, T. M., Andersen, J. N., and Olsen, O. H. (2000) Molecular dynamics simulations of protein-tyrosine phosphatase 1B. II. substrate-enzyme interactions and dynamics. *Biophys. J. 78*, 2191−2200.

(11) Bandyopadhyay, D., Kusari, A., Kenner, K. A., Liu, F., Chernoff, J., Gustafson, T. A., and Kusari, J. (1997) Protein-tyrosine phosphatase 1B complexes with the insulin receptor in vivo and is tyrosine-phosphorylated in the presence of insulin. *J. Biol. Chem. 272*, 1639−1645.

(12) Dadke, S., Kusari, J., and Chernoff, J. (2000) Down-regulation of insulin signaling by protein-tyrosine phosphatase 1B is mediated by an N-terminal binding region. *J. Biol. Chem. 275*, 23642−23647.

(13) Goldstein, B. J., Bittner-Kowalczyk, A., White, M. F., and Harbeck, M. (2000) Tyrosine dephosphorylation and deactivation of insulin receptor substrate-1 by protein-tyrosine phosphatase 1B. Possible facilitation by the formation of a ternary complex with the Grb2 adaptor protein. *J. Biol. Chem. 275*, 4283−4289.

(14) Walchli, S., Curchod, M. L., Gobert, R. P., Arkinstall, S., and Hooft van Huijsduijnen, R. (2000) Identification of tyrosine phosphatases that dephosphorylate the insulin receptor. A brute force approach based on "substrate-trapping" mutants. *J. Biol. Chem. 275*, 9792−9796.

(15) Zabolotny, J. M., Bence-Hanulec, K. K., Stricker-Krongrad, A., Haj, F., Wang, Y. P., Minokoshi, Y., Kim, Y. B., Elmquist, J. K., Tartaglia, L. A., Kahn, B. B., and Neel, B. G. (2002) PTP1B regulates leptin signal transduction in vivo. *Dev. Cell 2*, 489−495.

(16) Cheng, A., Uetani, N., Simoncic, P. D., Chaubey, V. P., Lee-Loy, A., McGlade, C. J., Kennedy, B. P., and Tremblay, M. L. (2002) Attenuation of leptin action and regulation of obesity by protein tyrosine phosphatase 1B. *Dev. Cell 2*, 497−503.

(17) Elchebly, M., Payette, P., Michaliszyn, E., Cromlish, W., Collins, S., Loy, A. L., Normandin, D., Cheng, A., Himms-Hagen, J., Chan, C. C., Ramachandran, C., Gresser, M. J., Tremblay, M. L., and Kennedy, B. P. (1999) Increased insulin sensitivity and obesity resistance in mice lacking the protein tyrosine phosphatase-1B gene. *Science 283*, 1544−1548.

DOI: 10.1021/acs.biochem.6b01025
Biochemistry 2017, 56, 96−106

(18) Zhang, S., and Zhang, Z. Y. (2007) PTP1B as a drug target: recent developments in PTP1B inhibitor discovery. *Drug Discovery Today 12*, 373−381.
(19) Zhang, Z. Y., Maclean, D., Thieme-Sefler, A. M., Roeske, R. W., and Dixon, J. E. (1993) A continuous spectrophotometric and fluorimetric assay for protein tyrosine phosphatase using phosphotyrosine-containing peptides. *Anal. Biochem. 211*, 7−15.
(20) Ruzzene, M., Donella-Deana, A., Marin, O., Perich, J. W., Ruzza, P., Borin, G., Calderan, A., and Pinna, L. A. (1993) Specificity of T-cell protein tyrosine phosphatase toward phosphorylated synthetic peptides. *Eur. J. Biochem. 211*, 289−295.
(21) Wiesmann, C., Barr, K. J., Kung, J., Zhu, J., Erlanson, D. A., Shen, W., Fahr, B. J., Zhong, M., Taylor, L., Randal, M., McDowell, R. S., and Hansen, S. K. (2004) Allosteric inhibition of protein tyrosine phosphatase 1B. *Nat. Struct. Mol. Biol. 11*, 730−737.
(22) Krishnan, N., Koveal, D., Miller, D. H., Xue, B., Akshinthala, S. D., Kragelj, J., Jensen, M. R., Gauss, C. M., Page, R., Blackledge, M., Muthuswamy, S. K., Peti, W., and Tonks, N. K. (2014) Targeting the disordered C terminus of PTP1B with an allosteric inhibitor. *Nat. Chem. Biol. 10*, 558−566.
(23) Baskaran, S. K., Goswami, N., Selvaraj, S., Muthusamy, V. S., and Lakshmi, B. S. (2012) Molecular Dynamics Approach to Probe the Allosteric Inhibition of PTP1B by Chlorogenic and Cichoric Acid. *J. Chem. Inf. Model. 52*, 2004−2012.
(24) Whittier, S. K., Hengge, A. C., and Loria, J. P. (2013) Conformational motions regulate phosphoryl transfer in related protein tyrosine phosphatases. *Science 341*, 899−903.
(25) Belay, A., and Gholap, A. V. (2009) Determination of integrated absorption cross-section, oscillator strength and number density of caffeine in coffee beans by the integrated absorption coefficient technique. *Int. J. Phys. Sci. 4*, 722−728.
(26) Meier, S., Li, Y. C., Koehn, J., Vlattas, I., Wareing, J., Jahnke, W. G., Wennogle, L. P., and Grzesiek, S. (2002) Letter to the Editor: Backbone resonance assignment of the 298 amino acid catalytic domain of protein tyrosine phosphatase 1B (PTP1B). *J. Biomol. NMR 24*, 165−166.
(27) Krishnan, N., Krishnan, K., Connors, C. R., Choy, M. S., Page, R., Peti, W., Van Aelst, L., Shea, S. D., and Tonks, N. K. (2015) PTP1B inhibition suggests a therapeutic strategy for Rett syndrome. *J. Clin. Invest. 125*, 3163−3177.
(28) Grzesiek, S., Stahl, S. J., Wingfield, P. T., and Bax, A. (1996) The CD4 determinant for downregulation by HIV-1 Nef directly binds to Nef. Mapping of the Nef binding surface by NMR. *Biochemistry 35*, 10256−10261.
(29) Shao, Y., Molnar, L. F., Jung, Y., Kussmann, J., Ochsenfeld, C., Brown, S. T., Gilbert, A. T. B., Slipchenko, L. V., Levchenko, S. V., O'Neill, D. P., DiStasio, R. A., Jr., Lochan, R. C., Wang, T., Beran, G. J. O., Besley, N. A., Herbert, J. M., Lin, C. Y., Van Voorhis, T., Chien, S. H., Sodt, A., Steele, R. P., Rassolov, V. A., Maslen, P. E., Korambath, P. P., Adamson, R. D., Austin, B., Baker, J., Byrd, E. F. C., Dachsel, H., Doerksen, R. J., Dreuw, A., Dunietz, B. D., Dutoi, A. D., Furlani, T. R., Gwaltney, S. R., Heyden, A., Hirata, S., Hsu, C. P., Kedziora, G., Khalliulin, R. Z., Klunzinger, P., Lee, A. M., Lee, M. S., Liang, W., Lotan, I., Nair, N., Peters, B., Proynov, E. I., Pieniazek, P. A., Rhee, Y. M., Ritchie, J., Rosta, E., Sherrill, C. D., Simmonett, A. C., Subotnik, J. E., Woodcock, H. L., III, Zhang, W., Bell, A. T., Chakraborty, A. K., Chipman, D. M., Keil, F. J., Warshel, A., Hehre, W. J., Schaefer, H. F., III, Kong, J., Krylov, A. I., Gill, P. M. W., and Head-Gordon, M. (2006) Advances in methods and algorithms in a modern quantum chemistry program package. *Phys. Chem. Chem. Phys. 8*, 3172−3191.
(30) van Dijk, M., and Bonvin, A. M. J. J. (2010) Pushing the limits of what is achievable in protein-DNA docking: benchmarking HADDOCK's performance. *Nucleic Acids Res. 38*, 5634−5647.
(31) Wassenaar, T. A., van Dijk, M., Loureiro-Ferreira, N., van der Schot, G., de Vries, S. J., Schmitz, C., van der Zwan, J., Boelens, R., Giachetti, A., Ferella, L., Rosato, A., Bertini, I., Herrmann, T., Jonker, H. R. A., Bagaria, A., Jaravine, V., Guntert, P., Schwalbe, H., Vranken, W. F., Doreleijers, J. F., Vriend, G., Vuister, G. W., Franke, D., Kikhney, A., Svergun, D. I., Fogh, R. H., Ionides, J., Laue, E. D., Spronk, C., Jurksa, S., Verlato, M., Badoer, S., Dal Pra, S., Mazzucato, M., Frizziero, E., and Bonvin, A. M. J. J. (2012) WeNMR: Structural Biology on the Grid. *Journal of Grid Computing 10*, 743−767.
(32) Phillips, J. C., Braun, R., Wang, W., Gumbart, J., Tajkhorshid, E., Villa, E., Chipot, C., Skeel, R. D., Kale, L., and Schulten, K. (2005) Scalable molecular dynamics with NAMD. *J. Comput. Chem. 26*, 1781−1802.
(33) Brandao, T. A., Hengge, A. C., and Johnson, S. J. (2010) Insights into the reaction of protein-tyrosine phosphatase 1B: crystal structures for transition state analogs of both catalytic steps. *J. Biol. Chem. 285*, 15874−15883.
(34) Case, D. A., Berryman, J. T., Betz, R. M., Cerutti, D. S., Cheatham, T. E., III, Darden, T. A., Duke, R. E., Giese, T. J., Gohlke, H., Goetz, A. W., Homeyer, N., Izadi, S., Janowski, P., Kaus, J., Kovalenko, A., Lee, T. S., LeGrand, S., Li, P., Luchko, T., Luo, R., Madej, B., Merz, K. M., Monard, G., Needham, P., Nguyen, H., Nguyen, H. T., Omelyan, I., Onufriev, A., Roe, D. R., Roitberg, A., Salomon-Ferrer, R., Simmerling, C. L., Smith, W., Swails, J., Walker, R. C., Wang, J., Wolf, R. M., Wu, X., York, D. M., and Kollman, P. A. (2015) *AMBER 2015*, University of California, San Francisco.
(35) Towns, J., Cockerill, T., Dahan, M., Foster, I., Gaither, K., Grimshaw, A., Hazlewood, V., Lathrop, S., Lifka, D., Peterson, G. D., Roskies, R., Scott, J. R., and Wilkens-Diehr, N. (2014) XSEDE: Acclerating Scientific Discovery. *Comput. Sci. Eng. 16*, 62−74.
(36) Humphrey, W., Dalke, A., and Schulten, K. (1996) VMD: visual molecular dynamics. *J. Mol. Graphics 14*, 27−38.
(37) Han, B., Liu, Y., Ginzinger, S. W., and Wishart, D. S. (2011) SHIFTX2: significantly improved protein chemical shift prediction. *J. Biomol. NMR 50*, 43−57.
(38) Zhang, Z. Y., Puius, Y. A., Zhao, Y., Sullivan, M., Lawrence, D. S., and Almo, S. C. (1997) Identification of a novel aryl phosphate-binding site in PTP1B: Implications for inhibitor design. *FASEB J. 11*, A834−A834.
(39) Zhang, Z. Y. (2002) Protein tyrosine phosphatases: structure and function, substrate specificity, and inhibitor development. *Annu. Rev. Pharmacol. Toxicol. 42*, 209−234.
(40) Peters, G. H., Iversen, L. F., Andersen, H. S., Møller, N. P., and Olsen, O. H. (2004) Residue 259 in protein-tyrosine phosphatase PTP1B and PTPalpha determines the flexibility of glutamine 262. *Biochemistry 43*, 8418−8428.

DOI: 10.1021/acs.biochem.6b01025
Biochemistry 2017, 56, 96−106